

This document is confidential and is proprietary to the American Chemical Society and its authors. Do not copy or disclose without written permission. If you have received this item in error, notify the sender and delete all copies.

Interaction of Azole-based Environmental Pollutants with the Coelomic Hemoglobin from *Amphitrite ornata*: a Molecular Basis for Toxicity

Journal:	<i>Biochemistry</i>
Manuscript ID	bi-2017-00041d.R1
Manuscript Type:	Article
Date Submitted by the Author:	06-Apr-2017
Complete List of Authors:	McCombs, Nikolette; North Carolina State University, Department of Chemistry Moreno Chicano, Tadeo; University of Essex, School of Biological Sciences Carey, Leah; North Carolina State University, Department of Chemistry Franzen, Stefan; NC State University, Chemistry Hough, Michael; University of Essex, School of Biological Sciences Ghiladi, Reza; North Carolina State University, Department of Chemistry

SCHOLARONE™
Manuscripts

1
2
3
4
5
6
7 Interaction of Azole-based Environmental Pollutants
8
9
10
11 with the Coelomic Hemoglobin from *Amphitrite*
12
13
14
15
16 *ornata*: a Molecular Basis for Toxicity
17
18
19
20

21 *Nikolette L. McCombs*¹, *Tadeo Moreno-Chicano*², *Leiah M. Carey*¹, *Stefan Franzen*¹, *Michael A.*
22
23 *Hough*^{2,*} and *Reza A. Ghiladi*^{1,*}
24
25

26
27 ¹Department of Chemistry, North Carolina State University, Raleigh, North Carolina, 27695-
28
29 8204
30
31

32 ²School of Biological Sciences, University of Essex, Wivenhoe Park, Colchester, Essex, CO4
33
34 3SQ, UK
35
36
37

38 Manuscript Correspondence:
39 Prof. Reza A. Ghiladi
40 Department of Chemistry
41 North Carolina State University
42 Raleigh, NC 27695
43 (919) 513-0680 (phone)
44 (919) 515-8920 (fax)
45 E-mail: Reza_Ghiladi@ncsu.edu
46
47

48
49 Dr. Michael A. Hough
50 School of Biological Sciences
51 University of Essex
52 Wivenhoe Park, Colchester
53 CO4 3SQ, Essex, UK
54 Tel: +44 1206 873317
55 mahough@essex.ac.uk
56
57
58
59
60

Abbreviations

1
2
3
4
5
6 BIm, benzimidazole; Bta, benzotriazole; Compound I, two-electron oxidized heme center when
7
8 compared to the ferric form, commonly as an $\text{Fe}^{\text{IV}}=\text{O}$ porphyrin π -cation radical; Compound II,
9
10 one-electron oxidized heme center when compared to the ferric form, commonly as an $\text{Fe}^{\text{IV}}=\text{O}$ or
11
12 $\text{Fe}^{\text{IV}}-\text{OH}$; Compound ES, two-electron-oxidized state containing both a ferryl center [$\text{Fe}^{\text{IV}}=\text{O}$]
13
14 and an amino acid (tryptophanyl or tyrosyl) radical, analogous to Compound ES in cytochrome c
15
16 peroxidase; Compound RH, 'Reversible Heme' state of dehaloperoxidase, formed from the
17
18 decay of Compound ES in the absence of co-substrate; CT1, charge transfer 1; DFT, density
19
20 functional theory; DHP, dehaloperoxidase; hhMb, horse heart myoglobin; HS, high-spin; Im,
21
22 imidazole; Inz, indazole; LS, low-spin; POP, persistent organic pollutant; SCRR, single crystal
23
24 resonance Raman; TBP, 2,4,6-tribromophenol; TCP, 2,4,6-trichlorophenol; WT, wild-type; 4-
25
26 BP, 4-bromophenol; 5c, 5-coordinate; 6c, 6-coordinate.
27
28
29
30
31
32
33
34
35
36
37
38
39
40
41
42
43
44
45
46
47
48
49
50
51
52
53
54
55
56
57
58
59
60

1
2
3 **ABSTRACT:** The toxicities of azole pollutants that have widespread agricultural and industrial
4 uses are either poorly understood or unknown, particularly with respect to how infaunal
5 organisms are impacted by this class of persistent organic pollutant. To identify a molecular
6 basis by which azole compounds may have unforeseen toxicity on marine annelids, we examine
7 here their impact on the multifunctional dehaloperoxidase (DHP) hemoglobin from the terebellid
8 polychaete *Amphitrite ornata*. UV-visible and resonance Raman spectroscopic studies showed an
9 increase in the 6-coordinate low spin heme population in DHP isoenzyme B upon binding of
10 imidazole, benzotriazole, and benzimidazole (K_d values = 52, 82, and 110 μM , respectively),
11 suggestive of their direct binding to the heme-Fe. Accordingly, atomic resolution X-ray crystal
12 structures, supported by computational studies, of the DHP B complexes of benzotriazole (1.14
13 \AA), benzimidazole (1.08 \AA), imidazole (1.06 \AA), and indazole (1.12 \AA) revealed two ligand
14 binding motifs, one with direct ligand binding to the heme-Fe, and another where the ligand
15 binds in the hydrophobic distal pocket without coordinating the heme-Fe. Taken together, the
16 results demonstrate a new mechanism by which azole pollutants can potentially disrupt
17 hemoglobin function, thereby increasing our understanding of their impact on infaunal organisms
18 in marine and aquatic environments.
19
20
21
22
23
24
25
26
27
28
29
30
31
32
33
34
35
36
37
38
39
40
41
42
43
44
45
46
47
48
49
50
51
52
53
54
55
56
57
58
59
60

1
2
3 A number of persistent organic pollutants (POPs) are comprised of five-membered nitrogen
4 (N)-containing heterocyclic rings belonging to the azole class of compounds. Such compounds,
5
6 examples of which include benzotriazole (Bta), benzimidazole (BIm), indazole (Inz), and
7
8 imidazole (Im), as well as their derivatives, have found a number of industrial and agricultural
9
10 uses. Benzotriazoles have been used as UV absorbers to protect polymers from photochemical
11
12 degradation, and more recently as anticorrosive additives (e.g., in cooling and hydraulic fluids,
13
14 antifreeze products, dishwasher detergents).^{1, 2} Recalcitrant to wastewater treatment where
15
16 effluent concentrations are as high as 10 μM ,^{1, 3, 4} they have been detected in rivers, lakes and
17
18 groundwater with concentrations as high as 1032 ng/L for benzotriazole and 516 ng/L for
19
20 methylbenzotriazole, and have been reported as the fourth most common European groundwater
21
22 pollutant.⁵ Likewise, benzimidazole and its derivatives have been used both as fungicides for
23
24 crop protection (applied directly to soil or sprayed over fields),⁶⁻⁸ and as veterinary antiparasitic
25
26 drugs administered to livestock (cows, sheep, hogs),^{9, 10} where they have been shown to enter
27
28 into the environment primarily through excretion (urine or feces). Similarly, indazole¹¹ and
29
30 imidazole¹²⁻¹⁴ derivatives have a wide variety of industrial, pharmaceutical, and agricultural uses.
31
32 Importantly, no azole-containing compounds are on the EPA priority pollutant list, and as such
33
34 these and similar compounds are often overlooked as environmental contaminants.
35
36
37
38
39
40
41
42

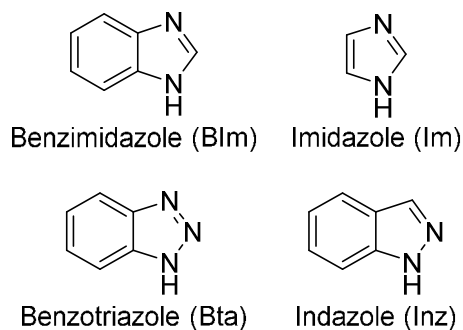
43
44 POPs enter marine and freshwater ecosystems through effluent releases, atmospheric
45
46 deposition, runoff, and other means, where their low water solubility results in strong binding to
47
48 particulate matter in aquatic sediments.¹⁵ As a result, sediments can serve as reservoirs or “sinks”
49
50 for azole POPs that lead to their exposure to sediment-dwelling organisms,⁹ either through
51
52 contact upon burrowing or via ingestion by deposit feeders. With very limited data available,
53
54 their persistence and fate in marine environments, as well as their toxicities to marine organisms,
55
56
57
58
59
60

1
2
3 are either unknown or poorly understood, with an added caveat that studies have shown that
4 some azole metabolites are more toxic than the parent compound.^{7, 16} Thus, as relatively little is
5 known regarding the underlying molecular basis for how infaunal systems are impacted by the
6 azole class of POPs, this lack of knowledge may lead to i) an underestimation of the
7 environmental toxicity of azole compounds that are currently in production or use, ii) approval of
8 other azole compounds for industrial or agricultural use despite their unknown potential for
9 harming marine environments, iii) limited cleanup or (bio)remediation efforts upon
10 environmental contamination due to a lack of concern regarding such compounds, and iv) a lack
11 of awareness of the individual or combined effects of POPs and their metabolites, particularly
12 with respect to their bioaccumulation, transport, and fate through environments where marine
13 annelid exposure is substantial. Thus, given their growing use across a breadth of applications, it
14 is of increasing importance to achieve a full understanding of how azole POPs and their
15 metabolites may impact marine environments.

16
17
18
19
20
21
22
23
24
25
26
27
28
29
30
31
32
33
34 Our platform for assessing the molecular basis by which azole compounds may have
35 unforeseen effects on infaunal organisms is the coelomic hemoglobin from the terebellid
36 polychaete *Amphitrite ornata*.¹⁷ In addition to its role in oxygen transport,¹⁷ this multifunctional
37 hemoprotein, historically named dehaloperoxidase (DHP) due to its ability to catalyze the
38 oxidative dehalogenation of 2,4,6-trihalophenols to their corresponding 2,6-dihaloquinones,¹⁸⁻²¹
39 is believed to have evolved in *A. ornata* to detoxify high levels of volatile organobromine
40 secondary metabolites secreted as repellents against predation by neighboring sediment-dwellers
41 in benthic ecosystems. In addition to this biologically-relevant peroxidase activity, the two
42 isoenzymes of DHP (A and B)²² have recently been shown to possess peroxygenase activity
43 against both native haloindole²³ and anthropogenic nitrophenol²⁴ substrates. As such, *A. ornata*

1
2
3 DHP represents a multifunctional catalytic globin that possesses a broad substrate scope with
4 activities commonly associated with the peroxidase and P450 families of enzymes.²⁵ Thus, given
5 its native peroxygenase activity against naturally-occurring halogenated indoles that are
6 structurally related to the aforementioned azole pollutants, questions thus arise as to whether
7 DHP binds, and/or potentially reacts with, similar compounds of anthropogenic origin, the
8 answers to which may potentially provide insight into previously unknown molecular
9 mechanisms for how infaunal organisms may be impacted by POPs.
10
11
12
13
14
15
16
17
18

19 To address these questions, here we have explored heterocyclic azole compounds,
20 comprising benzotriazole, benzimidazole, indazole and imidazole (Figure 1), for their ability to
21 bind to and possibly modulate the function of DHP. Using a combination of substrate binding
22 studies, biochemical assays, solution and crystal resonance Raman spectroscopy, and X-ray
23 crystallography, we have identified a previously unknown binding motif for azole compounds
24 with the hemoglobin of *A. ornata*. More importantly, however, the results demonstrate that there
25 may be a much larger number of heterocyclic compounds of anthropogenic origin that can bind
26 to marine hemoglobins, leading to a new mechanism by which pollutants can disrupt hemoglobin
27 function, a finding which may be important when assessing the environmental impact of
28 chemicals such as POPs and their metabolites on aquatic systems.
29
30
31
32
33
34
35
36
37
38
39
40
41
42



55
56
57
58
59
60

Figure 1. Azole ligands investigated for their binding to DHP.

EXPERIMENTAL

Materials and Methods. Reagent-grade chemicals (VWR, Sigma-Aldrich or Fisher Scientific) were used without further purification. Acetonitrile was HPLC grade. UV-visible spectroscopy was performed aerobically on a Varian Cary Bio50 spectrophotometer, or anaerobically on an Agilent 8454 diode-array spectrophotometer in a glovebox. Stock solutions (10-50 mM) of all compounds were prepared in MeOH, stored at 4 °C, and were periodically screened by HPLC to ensure that they had not degraded. Aliquots were stored on ice during use. Solutions of H₂O₂ were prepared fresh daily and kept on ice until needed. H₂O₂ concentration was determined by UV-vis ($\epsilon_{240} = 46 \text{ M}^{-1}\text{cm}^{-1}$).²⁶ DHP variants were expressed and purified as previously reported.²⁷⁻²⁹ Oxyferrous DHP was obtained by the aerobic addition of excess ascorbic acid to a solution of ferric DHP, followed by desalting (PD-10 column). Enzyme concentration was determined spectrophotometrically using $\epsilon_{\text{Soret}} = 116,400 \text{ M}^{-1}\text{cm}^{-1}$ for all isoenzymes.²⁸ Anaerobic studies were performed in an MBraun Labmaster 130 nitrogen-filled glovebox using Ar-degassed solutions of buffer, peroxide, substrate and enzyme.

Substrate-Binding Studies. Adapted from previously published protocols,³⁰ 50 mM azole stock solutions were prepared in 100 mM KP_i buffer (pH 7). The UV-visible spectrophotometer was first blanked using a solution of 10 μM ferric wild-type (WT) DHP B in buffer containing 10% MeOH. Difference spectra were then acquired in the presence of 2.5-100 eq. azole while maintaining both constant enzyme and MeOH concentrations. Analysis by nonlinear regression^{23, 24} using the GraFit software package (Erithacus Software Ltd.) of the experiments performed in triplicate provided a calculated A_{max} , which was in turn used to calculate α for the average ΔA for each substrate concentration. A nonlinear regression plot provided the reported

1
2
3 apparent K_d values.^{23, 24}
4
5

6 **Resonance Raman Studies.** Samples for solution resonance Raman spectroscopic studies
7
8 were prepared with final concentrations of 75 μ M WT DHP B and 3.75 mM azole in 100 mM
9
10 KP_i (pH 7 or 9) containing 10% MeOH (v/v), and then transferred to a 5-mm o.d. glass NMR
11
12 tube. Anaerobic samples were prepared inside a glovebox in the same fashion using septum
13
14 capped NMR tubes. Spectra were obtained by Soret band excitation (400-430 nm; 60 mW
15
16 power) as previously described.²³
17
18

19
20 In order to validate the ligand states in DHP-azole crystals, additional single crystal
21
22 resonance Raman data (SCRR) were measured, from separate crystals, using the on-line MS3
23
24 microspectrophotometer³¹ at the Swiss Light Source beamline X10SA with an excitation
25
26 wavelength of 405 nm. Raman shifts were calibrated using 4-acetaminophen as reference, and all
27
28 data were analysed using the SLS-APE³² in-house suite. Several RR spectra were measured from
29
30 each crystal prior to X-ray exposure in order to test for laser-induced photoreduction of the
31
32 heme-Fe. Averaged, accumulated spectra were measured for each DHP-azole crystal prior to,
33
34 and following, measurement of X-ray data (diffraction data not shown).
35
36
37

38
39 **Protein Crystallization and X-ray Diffraction Studies.** Crystals of non His-tagged
40
41 recombinant DHP B²⁴ were obtained through the hanging-drop vapor diffusion method: 12
42
43 mg/mL DHP B in 20 mM Na cacodylate (pH 6.4) was mixed with a reservoir solution
44
45 comprising 14-20% (w/v) PEG 4000 and 150-250 mM ammonium sulfate. Drops were prepared
46
47 using 1:1 and 1:2 protein:reservoir ratios, obtaining final drop volumes of 4 and 6 μ L,
48
49 respectively. Crystals grew at 4 °C in 3-6 days. DHP B ferric crystals were soaked in reservoir
50
51 solutions supplemented with either imidazole (5 mM) or indazole, benzimidazole or
52
53 benzotriazole (10 mM, each in 2% DMSO). Crystals were soaked for 5-10 min, before transfer to
54
55
56
57
58
59
60

1
2
3 a cryo-solution containing reservoir solution supplemented with 20% glycerol prior to flash-
4
5 freezing in liquid nitrogen.
6
7

8 Data were measured to atomic resolution for DHP B ligand complexes using Diamond Light
9
10 Source beamline I04-1. Data measured at Diamond were processed automatically in Xia2 using
11
12 XDS³³ and Aimless³⁴ with the resolution limit based on a criterion of $CC^{1/2} > 0.5$ for the highest
13
14 resolution shell. Data from SLS were manually processed using XDS and Aimless using the
15
16 same criteria. Structures were refined by maximum likelihood methods in Refmac5 within the
17
18 CCP4 suite using the CCP4i2 GUI. Ligands were modelled into strong sigmaA-weighted Fo-Fc
19
20 electron density features with ligand chemical structures and restraints taken from the HIC-UP³⁵
21
22 database (Uppsala) and from SMILES. Validation of structures utilised MolProbity³⁶, the JCSG
23
24 Quality Control Server and the PDB validation server. Coordinates and structure factors were
25
26 deposited in the RCSB Protein Data Bank with accession codes given in Table S1. Absorbed X-
27
28 ray doses were determined using Raddose 3D.³⁷
29
30
31
32
33

34 **Computational Methodology.** All calculations were performed using the *Gaussian 09*
35
36 software package. Structures were optimized in the low spin doublet state in vacuum utilizing the
37
38 B3LYP functional and 6-31G* basis set for C, N, O, H and the double- ζ basis set of Schafer et
39
40 al.,³⁸ enhanced with an extra p function (exponent 0.134915) on Fe. The geometry optimized
41
42 structures were carried out until reaching an energy difference of 10^{-8} Ha on successive iterations
43
44 without constraints. A protoporphyrin IX model was employed that replaced the propionate arms
45
46 with methyl groups, and the proximal histidine with a methylimidazole axial ligand.
47
48
49
50
51
52
53
54
55
56
57
58
59
60

RESULTS

UV-visible Spectroscopic Studies. The electronic absorption spectra in 100 mM KP_i (pH 7) containing 10% MeOH (v/v) at 25 °C for ferric DHP B alone [407 (Soret), 507, 540 (sh), 635 nm; black] and in the presence of 100 eq. Im [416 (Soret), 537, 565 nm; pink], Bta [418 (Soret), 541, 575 (sh); blue], BIm [410 (Soret), 537, 565 (sh); green], and Inz [408 (Soret), 506, 635 nm; red] are shown in Figure 2A. Relevant spectral features and analysis are found in Table 1, and additional discussion supporting the oxidation state assignment of the DHP-azole adducts as containing 6cLS *ferric* hemes (as opposed to 6cLS *ferrous*) can be found in the Supporting Information.

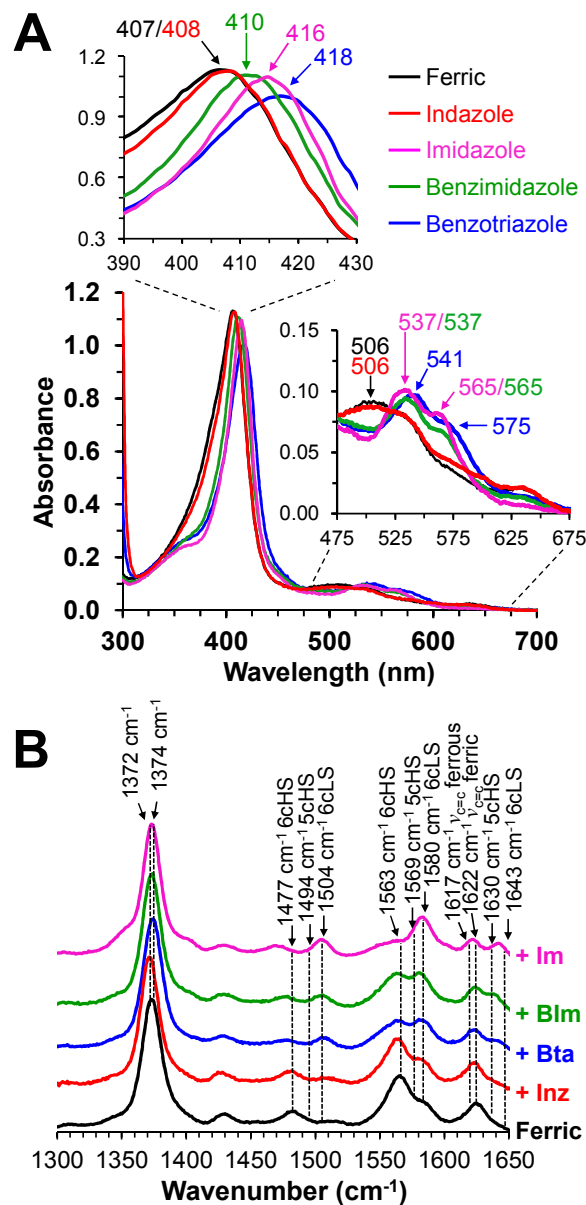


Figure 2. (A) UV-visible spectra of WT ferric DHP (10 μM , black) in the presence of 100 equiv. of imidazole (pink), benzimidazole (green), benzotriazole (blue), and indazole (red) in 10% MeOH/100 mM KPi (v/v) at pH 7. (B) Resonance Raman spectra of DHP-azole complexes as in panel A at 75 μM enzyme and 50 equiv. azole.

Table 1. UV-visible spectroscopic data for WT DHP B and its azole adducts.^a

	λ_{\max} (nm)	A_{Soret}/A_{380}	A_{614}/A_{645}
DHP B	407 (Soret), 507, 540 (sh), 635	1.86	1.11
+imidazole (Im)	416 (Soret), 537, 565	3.74	1.64
+benzotriazole (Bta)	418 (Soret), 541, 575 (sh)	3.04	1.34
+benzimidazole (BIm)	410 (Soret), 537, 565 (sh)	3.05	1.16
+indazole (Inz)	408 (Soret), 506, 635	2.08	1.08

^a 10% MeOH (v/v) in 100 mM KP_i, pH 7, 25 °C, 100 equiv. azole.

The shifts in the relative populations of 5-/6-coordinate (5c/6c) high-/low-spin (HS/LS) heme species in DHP B caused by azole binding can be demonstrated by analysis of the A_{Soret}/A_{380} and A_{614}/A_{645} ratios^{29, 39, 40}: the presence of the azole led to an increase in the A_{Soret}/A_{380} ratio, from ~3.04 for DHP-Bta and DHP-BIm, to as high as 3.74 for DHP-Im, versus 1.86 for WT DHP B alone. Similarly, the A_{614}/A_{645} ratio was also increased per the trend Im > Bta > BIm > Inz ≈ DHP B. Taken together, for Bta, BIm, and Im, the bathochromic shifts observed upon ligand binding (as revealed by the A_{Soret}/A_{380} ratio) and loss of the charge transfer (CT1) feature (highlighted by the A_{614}/A_{645} ratio) were suggestive of a 6cLS heme in DHP. Notably, indazole binding did not significantly alter the spectral features of the starting ferric enzyme. Overall, these UV/vis spectroscopic results for azole binding are in good agreement with the interpretations provided by resonance Raman spectroscopy (vide infra).

Additionally, a pH-dependence on the spectral features consistent with the known alkaline transition⁴¹ in DHP was observed at pH 9 in the absence of the azole ligands [415 (Soret), 546, 565 (sh)] and in their presence: Im [417 (Soret), 537, 565 (sh)], Bta [421 (Soret), 546, 577 (sh)], BIm [416 (Soret), 546, 577 (sh)], and Inz [415 (Soret), 546, 577 (sh)] (Figure S2). *Qualitatively*, the magnitude of the spectral shifts at pH 9 and their interpretation follow the same trends as pH 7 (Bta > Im > BIm >> Inz).

1
2
3 **Solution Resonance Raman Studies.** Resonance Raman spectra obtained aerobically in 100
4 mM KP_i (pH 7) containing 10% MeOH (v/v) at 25 °C are shown in Figure 2B for ferric WT
5 DHP B (75 μM ; black) alone and in the presence of 50 equiv of Im (pink), Bta (blue), BIm
6 (green), and Inz (red), with features reported in Table S2. The DHP core size marker bands ν_3
7 (1470 – 1510 cm^{-1}) and ν_2 (1560 – 1580 cm^{-1}) represent the population distribution of six
8 coordinate vs. five coordinate heme species, respectively, and are sensitive to spin state.⁴² For
9 WT DHP B in the absence of an azole ligand, the presence of 10% MeOH in the buffer solution
10 leads to an increase in the 6cHS heme-Fe population (to nearly 100%) when compared to
11 aqueous buffer that is normally a mixture of 5cHS and 6cHS metaquo heme.⁴³ This shift due to
12 the presence of MeOH has been attributed to a destabilization of the distal histidine (His⁵⁵) in the
13 solvent exposed (or “open”) conformation in the 10% MeOH buffer solution.²³
14
15
16
17
18
19
20
21
22
23
24
25
26
27
28
29

30 The following observations were noted for DHP B in the presence of an azole ligand:
31 imidazole yielded the greatest shift in the DHP heme core size marker bands, from that of a
32 6cHS spectrum ($\nu_3 = 1477 \text{ cm}^{-1}$, $\nu_2 = 1563 \text{ cm}^{-1}$; black) to one that reflects 6cLS ($\nu_3 = 1504 \text{ cm}^{-1}$;
33 $\nu_2 = 1580 \text{ cm}^{-1}$; $\nu_{10} = 1643 \text{ cm}^{-1}$; pink). Specifically, the DHP-Im ν_3 LS band was seen at 1504
34 cm^{-1} with a small abundance of ν_3 HS at 1471 cm^{-1} , while the ν_2 LS band was noted at 1581 cm^{-1}
35 with a small shoulder representing the weak abundance of the ν_2 HS band. A slight shoulder at
36 $\sim 1350 \text{ cm}^{-1}$ and an increase at 1617 cm^{-1} corresponding to the $\nu_{c=c}$ ferrous core size marker band
37 both suggest a minor reduction of DHP occurs in the presence of imidazole that was not
38 observable by UV-visible spectroscopy. With the exception of these ferrous components, the
39 features of DHP-Bta and DHP-BIm were similar to those observed with DHP-Im: core size
40 marker bands were observed at $\sim 1505 \text{ cm}^{-1}$ and $\sim 1581 \text{ cm}^{-1}$, with small scattering for the HS
41 features for both azole adducts. Overall, these three azole ligands yielded spectral features in
42
43
44
45
46
47
48
49
50
51
52
53
54
55
56
57
58
59
60

1
2
3 DHP that are consistent with other ferric LS hemoprotein adducts of DHP⁴⁴, horseradish
4 peroxidase⁴⁴, horse heart myoglobin⁴⁴, and P450_{BM3}⁴⁵⁻⁴⁷ (Table S2). Finally, while the presence
5
6 of Im, Bta, and BIm led to a significant shift from a primarily 6cHS heme in DHP to a 6cLS one,
7
8 DHP-Inz exhibited little to no LS features apart from the typical distribution for WT DHP alone,
9
10 in agreement with the UV/vis spectroscopic studies (vide supra).
11
12

13
14
15 In contrast to the 6cLS heme formed upon azole binding, other DHP substrates lead to a
16
17 5cHS ferric heme: the 4-halophenol series,^{19, 48} 5-substituted haloindoles,²³ 4-nitrophenol²⁴ and
18
19 4-nitrocatechol²⁴ all have known binding sites inside the distal pocket that displace the distal
20
21 His⁵⁵ to the 'open' conformation (Figure S3A), thereby destabilizing the iron-bound water
22
23 ligand, and yielding a 5cHS ferric heme. None, however, bind directly to the iron. Thus, the
24
25 observation of a 6cLS heme for DHP complexes of Im, Bta, and BIm strongly suggests that these
26
27 three ligands are binding directly to the heme-iron, in agreement with the ligand binding motif
28
29 revealed by X-ray crystallography (vide infra).
30
31
32

33
34 Two additional resonance Raman studies were performed: i) spectra were obtained
35
36 anaerobically at pH 7 (Figure S4), and showed no significant differences when compared to the
37
38 aerobic ones; ii) spectra collected aerobically at pH 9 (Figure S5) were similar to those observed
39
40 at pH 7, with only minor differences that were attributable to the known acid-alkaline transition⁴¹
41
42 in DHP.
43
44

45
46 **Ligand Binding Studies.** Using the observed hypochromicity and bathochromic shift of the
47
48 Soret band upon ligand binding, optical difference spectra were recorded as a function of azole
49
50 concentration (2.5-100 eq; Figure S6) to determine the apparent dissociation constants (K_d). The
51
52 K_d values for Im, Bta, and BIm were within ~2-fold of each other (52–110 μ M, Table 2). As Inz
53
54 showed no significant optical changes, no K_d value was determined. When compared to the
55
56
57
58
59
60

naturally-occurring haloindole peroxygenase substrate 5-Br-indole (150 μM), the three azoles showed higher affinities for DHP, although the comparison is mixed for the other 5-substituted halogenated indoles (5-I-indole: 62 μM ; 5-Cl-indole: 317 μM) that are not native to benthic environments.²³ The binding affinities for the three azoles were also on a par with, or slightly stronger, than the anthropogenic 4-nitrophenol (262 μM), 2,4-dinitrophenol (105 μM) and 4-nitrocatechol (40 μM) substrates,²⁴ and were significantly lower than that for the native 4-bromophenol (1.15 mM ⁴³), a known inhibitor⁴⁹ of the enzyme. Additional discussion of the binding affinity of the azoles as informed by X-ray crystallography can be found below.

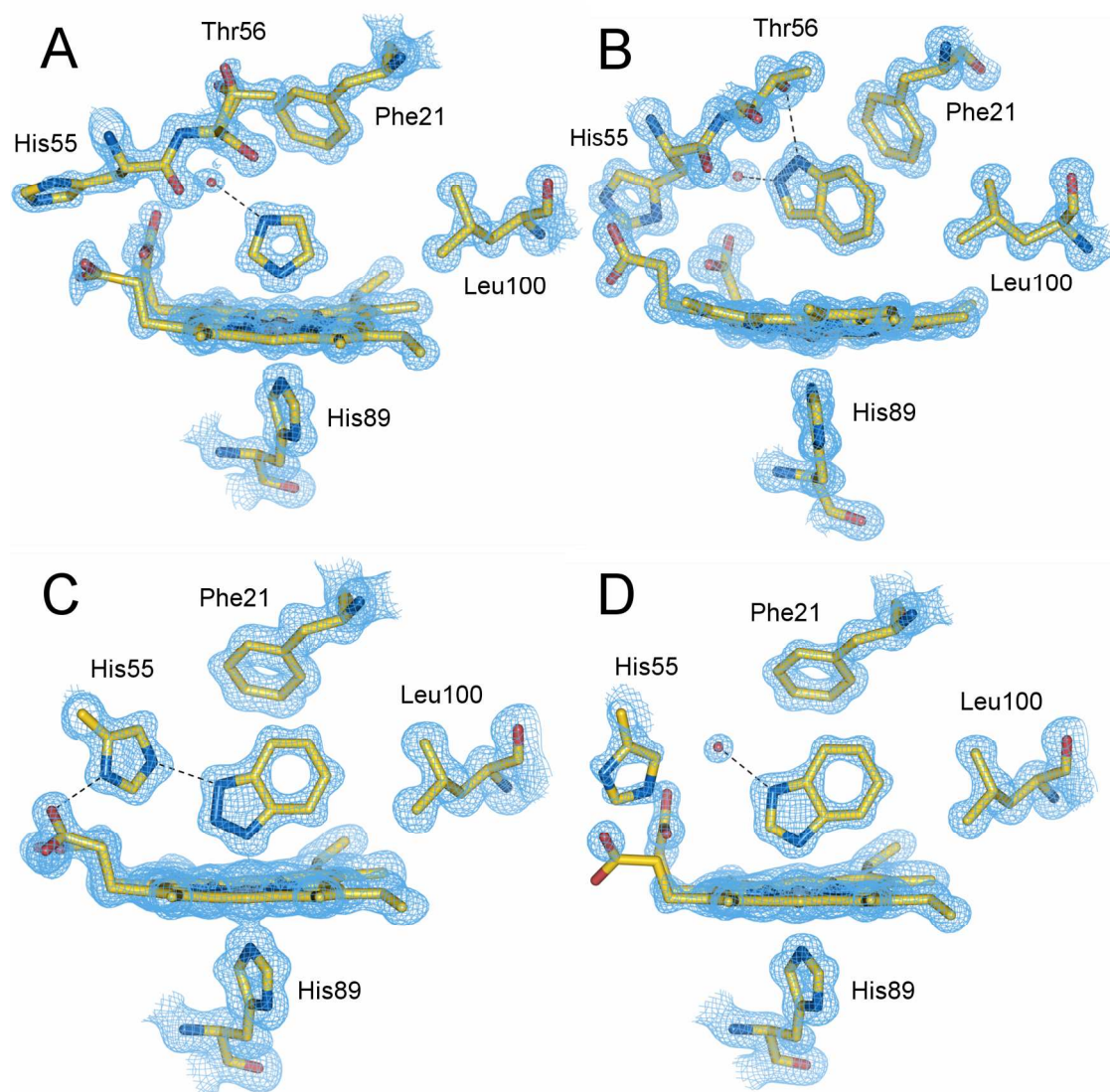
Table 2. K_d Values for Ligand Binding to Ferric DHP B at pH 7.

Ligand	K_d (μM), pH 7	Ref.
Azole		
imidazole (Im)	52 ± 2	a
benzotriazole (Bta)	82 ± 2	a
benzimidazole (BIm)	110 ± 8	a
indazole (Inz)	n. d. ^b	a
Indole		
5-I-indole	62 ± 10	23
5-Br-indole	150 ± 10	23
5-Cl-indole	317 ± 23	23
Phenol		
4-nitrocatechol	40 ± 1	24
2,4-dinitrophenol	105 ± 21	24
4-nitrophenol	262 ± 23	24
4-Br-phenol	1150	43

^a this work, ^b n. d. = not determinable due to lack of spectral changes.

X-ray Crystallographic Studies of DHP B Complexed with Azoles. Crystal structures were determined to atomic resolution for all four azole ligands. Data collection and refinement statistics are found in Table S1. Additional single crystal resonance Raman data conducted on crystals prepared in the same manner identified all crystals as being initially in the ferric state, with rapid conversion to the ferrous form following X-ray exposure (vide infra). In each case,

1
2
3 full occupancy ligand binding was observed in at least one molecule of the DHP B dimer, and
4 the relevant discussion below is thus limited to the results for the best defined ligand sites. All
5
6 the relevant discussion below is thus limited to the results for the best defined ligand sites. All
7
8 ligands were found in the distal heme pocket, and interacted directly with the iron with the
9
10 exception of indazole. A comparison of the different binding environments for each ligand is
11
12 shown in Figure 3, and selected Fe-ligand distances can be found in Table 3.
13
14
15
16
17



55 **Figure 3.** Comparison of the different binding modes at the DHP heme active site by (A)
56 imidazole, (B) indazole, (C) benzotriazole and (D) benzimidazole. Note that in panel (A) only
57 one of two partial occupancy waters that hydrogen bond to imidazole is shown for clarity.
58
59
60

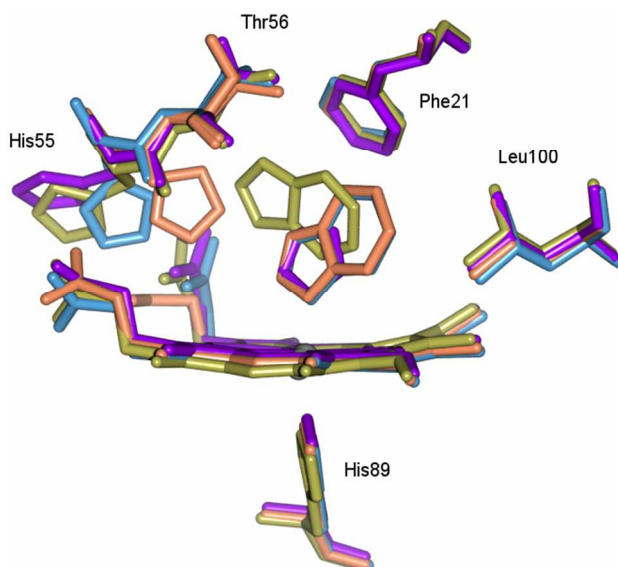
Table 3: Heme iron-ligand distance for each complex and hydrogen bonds observed.

Complex	K_d (μM) pH 7 ^a	Fe-ligand distance (\AA)	Hydrogen bonds (\AA)			
			H ₂ O- ligand	H ₂ O- propionate	H ₂ O- Tyr38	Ligand- His55
Imidazole	52 ± 2	2.02	2.76/2.89 ^b	2.87/4.23	-	-
Benzotriazole	82 ± 2	2.05	-	-	-	2.65
Benzimidazole	110 ± 8	2.05	2.78	2.88	-	-
Indazole	n. d. ^c	3.94	2.57	2.63	2.50	-

^a from Table 2; ^b values given for monomers A & B; ^c n. d. = not determinable due to lack of spectral changes

For DHP-Im (Figure 3A), the imidazole ligand is observed with full occupancy in both of the active sites of the dimer in the asymmetric unit. It forms a hydrogen bond with a water molecule in the pocket (this water occupies a single position in monomer B, or two alternate partial occupancy water positions in monomer A) and coordinates the iron (Table 3), with His⁵⁵ swung out of the distal pocket. In DHP-Bta (Figure 3C), the benzotriazole ligand interacts directly with the iron at the heme distal pocket, and is stabilized by forming a 2.65 \AA hydrogen bond with the N ^{ϵ 2} atom of His⁵⁵, which is swung fully into the pocket. Benzotriazole is found in just one of the active sites (monomer B), while in the other one we observe a hemichrome species with His⁵⁵ interacting with the iron and forming a hexacoordinated complex (data not shown). For the DHP-BIm adduct (Figure 3D), the benzimidazole ligand also complexes the heme-iron in the axial position resulting in a hexacoordinate species, and forms a hydrogen bond with a water present in the pocket. Benzimidazole is found in both active sites with good occupancy. For all the double ring aromatic ligands, residues Phe 21, Phe 35, Val 59 and Leu 100 provide a hydrophobic environment in the pocket to favour their binding. A superposition of the DHP-Im, DHP-BIm and DHP-Bta binding modes, together with the positioning of indazole in the pocket, is given in Figure 4. The ligands superimpose well, albeit with the smaller Im being rotated slightly away from His⁵⁵. The residues forming the hydrophobic pocket Phe24, Phe35, Val59,

1
2
3 Leu100, are in near-identical orientations in all three structures. Notably, for Bta and BIm, Phe21
4
5 is forced to rotate $\sim 13^\circ$ away from the heme in order to accommodate the larger ligand. A shift in
6
7 the protein backbone occurs in the DHP-Bta structure, likely the result of the hydrogen bond
8
9 formation between His55 and the bound ligand.
10
11



12
13
14
15
16
17
18
19
20
21
22
23
24
25
26
27
28
29
30
31
32 **Figure 4.** Superposition of the active site for the azole-DHP complexes, showing the binding
33 environment with the most relevant residues in each case. Imidazole is shown in purple, indazole
34 in gold, benzimidazole in blue, and benzotriazole in orange.
35
36

37
38 In contrast, in the case of DHP-Inz (Figure 3B), the indazole ligand is found with full
39 occupancy in the distal pocket, but does not complex the heme-iron. Rather, it is located more
40 distant from the heme plane than the other ligands, and presents hydrogen bond interactions with
41 Thr⁵⁶-O^{γ1} and a neighbouring water molecule. It also has a hydrophobic stacking interaction with
42 the aromatic ring of Phe 21, with the ring planes close to parallel and separated by ~ 4 Å. Overall,
43 the ligand binding motif in DHP-Inz is in good agreement with the observations noted above for
44 both UV-visible and resonance Raman spectroscopies that suggested a HS heme persists in DHP
45 even in the presence of the indazole ligand.
46
47
48
49
50
51
52
53
54
55

56
57 Single crystal resonance Raman data were measured from separate DHP-azole crystals
58
59
60

1
2
3 (Figure S7 and Table S3), grown and soaked in the same manner as described above, in order to
4 facilitate comparison with solution data and to monitor redox and ligand states. The 5c ferric
5 heme in DHP-Inz crystals was highly susceptible to photoreduction by the 405 nm excitation
6 laser, while the 6c hemes of the remaining complexes were not, provided that relatively low laser
7 powers were used. All crystals underwent rapid reduction in the X-ray beam consistent with
8 previous reports on cryo-radiolytic reduction of heme proteins.⁵⁰ This suggests that the DHP-
9azole structures represent a mixture of ferric and (predominantly) ferrous hemes.

10
11
12
13
14
15
16
17
18
19
20 **Computational Studies.** To investigate azole binding and the possible ligation with the
21 heme Fe, a density functional theory (DFT) computational approach was utilized. All structures
22 converged to the binding of the free azole nitrogen to the iron, as seen in Figure S8 and Table S4.
23 For Bta, there are two possible binding conformations (Figure S8D and E) that are < 1 kcal/mol
24 different in energy, however the binding through the N2 nitrogen is stronger (Fe-N distance of
25 2.038 Å) versus 2.087 Å through N3. The crystal structure shows only one binding conformation
26 for Bta (Figure 3C) that matches closely to the calculated conformation in Figure S8D. The
27 imidazole DFT structure showed coordination to the iron through N2 with a Fe-N distance of
28 2.04 Å (Figure S8A), which matches nicely with the crystal structure (Figure 3A). BIm also
29 showed heme ligation through BIm N2 with an Fe-N distance of 2.040 Å (Figure S8B) that
30 matches well with the observed crystal structure (Figure 3D). Indazole was calculated to bind in
31 a similar fashion to the Bta conformation (Figure S8C and E, respectively), but in the crystal
32 structure is shown to bind in the distal pocket ~4.0 Å away and not directly coordinate to the
33 heme iron (Figure 3B). Bta (E) and Inz (C) likely do not bind in these conformations due to
34 steric effects with other residues inside the distal pocket (Figure S9, see Discussion below).

35
36
37
38
39
40
41
42
43
44
45
46
47
48
49
50
51
52
53
54
55 **Biochemical Assays.** The azoles were explored as possible peroxidase/peroxygenase
56
57
58
59
60

1
2
3 substrates for DHP (see Supporting Information for experimental details). However, HPLC
4
5 analysis revealed that under all conditions tested (variable pH, variable H₂O₂ concentration), no
6
7 oxidation nor degradation of these compounds was noted (data not shown). Further, stopped-
8
9 flow UV-visible spectroscopic studies of the two high-valent iron-oxo species typically invoked
10
11 in hemoprotein reactions, Compounds I²⁹ and ES²⁷, when pre-formed and reacted with 10-100
12
13 eq. of azole, showed that neither were able to oxidize the azoles (data not shown).
14
15

16
17 Given their K_d values of ~50-110 μM , the azoles were explored as possible inhibitors of
18
19 peroxygenase activity: 10 μM ferric WT DHP B was preincubated with 50-750 mol equivalents
20
21 azole, reacted with 50 eq. each of 5-bromoindole and H₂O₂, and then subjected to HPLC
22
23 analysis. Substrate conversion of 5-bromoindole was uninhibited over the azole concentration
24
25 range analyzed. This differs from the known inhibitor⁴⁹ 4-bromophenol ($K_d = 1.15 \text{ mM}^{43}$) that
26
27 inhibits both peroxygenase and peroxidase activities. We rationalize this counterintuitive result
28
29 by the following: the weaker binding 4-bromophenol inhibitor binds internally in the distal
30
31 pocket (without directly ligating the heme iron), thereby inhibiting substrate binding. On the
32
33 other hand, although Im, Bta, and BIm directly coordinate to the iron, the binding of H₂O₂ is
34
35 stronger: we estimate the K_d of H₂O₂ to have an upper bound equal to the $K_M^{H_2O_2}$ value of 35 μM
36
37 (from Michaelis-Menten kinetics: if $k_1 \ll k_{-1}$, then $K_M = K_d$; if $k_1 \geq k_{-1}$, then $K_M > K_d$).
38
39 Therefore, H₂O₂ is able to displace the coordinated azole ligands, allowing for both enzyme
40
41 activation and substrate turnover.
42
43
44
45
46
47
48
49
50

51 DISCUSSION

52
53 Given its native peroxygenase activity against naturally-occurring halogenated indoles, the
54
55 aim of the present study was to explore if DHP is able to bind, and/or potentially react with,
56
57
58
59
60

1
2
3 structurally related compounds of anthropogenic origin. Typically, inhibitors of O₂ transport in
4 hemoglobins are small molecules (e.g. carbon monoxide, cyanide, azide, nitric oxide) owing to
5 the lack of an active site pocket capable of allowing access to facilitate binding of larger
6 ligands.⁵¹ As such, larger N-containing heterocyclic compounds, such as those found in the
7 azoles investigated here, would not be considered as ligands capable of binding in a globin active
8 site, let alone coordinate to the heme-iron. However, owing to its multifunctional nature as a
9 detoxification enzyme that is unrelated to its primary function as an O₂ transport globin, DHP
10 possesses an active site pocket capable of halophenol and haloindole binding that supports both
11 peroxidase and peroxygenase activities, respectively.²⁵

12
13 We have previously postulated that when one considers the known substrate binding sites for
14 halophenols, haloindoles, and nitrophenols in DHP, there is evidence to suggest at least two
15 different substrate binding motifs (Figure S3B).²⁵ The first binding motif is observed for the
16 peroxidase substrates 2,4,6-tribromophenol (TBP) and 2,4,6-trichlorophenol (TCP): both TBP
17 (in WT DHP A)⁵² and TCP [in the DHP A(Y34N) mutant]⁵³ deeply bind in the distal cavity near
18 the α edge of the heme in close proximity to L100, the substrates (but not the bromine atoms)
19 encompass the Xe binding site, the phenolic-OH is pointed towards the heme Fe, and the
20 substrate is far enough removed that His⁵⁵ is found in both the ‘open’ and the ‘closed’ (internal)
21 conformations.^{42, 43} The second motif is observed for 4-nitrophenol, 4-nitrocatechol, and the 4-
22 halophenol series: these substrates bind above the heme with a tilt away from the β edge, the
23 aromatic rings are oriented for π -stacking interactions with F21, the halogen and nitro
24 substituents of the phenolic substrates are positioned internally in the Xe1 binding site, the
25 phenolic-OH is situated near the pocket entrance with stabilizing H-bonding interactions to the
26 heme propionate D and/or Y38, and the distal histidine (His55) is swung into the solvent exposed
27
28
29
30
31
32
33
34
35
36
37
38
39
40
41
42
43
44
45
46
47
48
49
50
51
52
53
54
55
56
57
58
59
60

1
2
3 ‘open’ conformation.²⁴ TCP has also been shown to bind in an alternate orientation in the DHP
4
5 A(Y34N/S91G) double mutant that more closely resembles this second binding motif: situated at
6
7 the heme γ edge between both heme propionate arms, the phenolic-OH hydrogen bonds to Y38,
8
9 the Cl substituent of the C4 carbon points toward the heme-Fe, and His⁵⁵ is found in the ‘open’
10
11 conformation.⁵³
12
13

14
15 In the case of the azole compounds Bta, BIm, and Im, a third ligand binding motif is now
16
17 identified, one in which the ligand binds directly to the heme-Fe through a coordinate covalent
18
19 bond from a nitrogen atom, resulting in a hexacoordinate low spin (6cLS) adduct. Such a direct
20
21 ligation of N-heterocyclic compounds to heme proteins has been previously studied in the
22
23 cytochrome P450 monooxygenases: organic building blocks such as imidazoles and triazoles,
24
25 among other azole derivatives found in pharmaceuticals, have been shown to coordinate directly
26
27 to heme iron through the nitrogen, termed type II binding ligands.⁵⁴ The binding of azole
28
29 compounds to P450s has been shown to be inhibitory owing to the change in spin and
30
31 coordination state from a 5cHS to a 6cLS heme, thus making it more difficult for reduction to
32
33 take place to initiate the P450 catalytic cycle.^{54, 55} In the case of DHP, the azole derivatives that
34
35 were explored in this work also lead to this spin state shift upon their binding, resulting in
36
37 significant optical changes similar to those observed with the P450s. However, unlike the
38
39 inhibition that is seen with the P450s in the presence of azole compounds, there is no hindrance
40
41 on the peroxidase and peroxygenase activities of DHP as such an initial reduction is not invoked
42
43 in the DHP peroxidase/peroxygenase catalytic cycles. Rather, binding of H₂O₂ likely displaces
44
45 the azole ligands, leading to enzyme activation via the resulting reactive ferryl species.
46
47
48
49
50
51
52

53 The DFT computational results, performed in the absence of the protein using a model heme,
54
55 support a direct ligation of all four azole compounds to the heme iron. In the case of imidazole
56
57
58
59
60

1
2
3 and benzimidazole, the calculated binding through the N3 nitrogen is in good agreement with
4 that observed by X-ray crystallography. For benzotriazole, two different binding geometries of
5
6 that observed by X-ray crystallography. For benzotriazole, two different binding geometries of
7
8 nearly degenerate energy were calculated, one through the N2 nitrogen, the other through N3.
9
10 However, the crystallographically observed ligand binding geometry matches that of the N2
11
12 conformation, likely due to steric hindrance with the protein that occurs with the more ‘vertical’
13
14 orientation of the azole ligand (Figure S9). Interestingly, indazole was also calculated to bind
15
16 through the N2 nitrogen in this ‘vertical’ arrangement owing to protonation at N1 (the 1-H
17
18 tautomer of indazole is 15.1 kJ/mol more stable than the 2-H tautomer⁵⁶), but was found to not
19
20 bind directly through either nitrogen by X-ray crystallography; rather, indazole binding in the
21
22 hydrophobic pocket more closely resembles the second motif described above for 4-nitrophenol,
23
24 4-nitrocatechol, and the 4-halophenol series. We surmise that the observed binding orientation
25
26 of indazole in the DHP active site pocket must be more favorable than the annular
27
28 tautomerization needed for N1 binding and direct ligation to the heme iron, with steric hindrance
29
30 precluding the ‘vertical’ binding arrangement required for N2 binding (Figure S9).
31
32
33
34
35

36 Consistent with the postulate that small-molecule binding sites may exist with regulatory
37
38 implications in DHP, we have put forth that both the conformational flexibility (‘open’ vs.
39
40 ‘closed’, Figure S3A) and the tautomeric state of the distal histidine, His⁵⁵, may govern how
41
42 DHP switches between its hemoglobin and enzymatic activities upon substrate binding.^{48, 57-60}
43
44 Although the azoles themselves are not substrates, this conformational flexibility of the distal
45
46 histidine is well-highlighted from the distances between Fe and His⁵⁵ of the four azole-bound
47
48 structures of DHP, from the fully ‘open’ conformation of DHP-Im (9.47 Å), to the progressively
49
50 more ‘closed’ structures of DHP-Inz (8.54 Å), DHP-BIm (7.11 Å), and DHP-Bta (5.93 Å),
51
52
53
54
55
56
57
58
59
60
Figure 4 (note: the shorter of the Fe-N^{ε2} or Fe-N^{δ1} distances is given, or in the case of DHP-BIm,

1
2
3 Fe-C^{δ2}). The movement of His55 encompasses a side chain reorientation but also a shift of the
4
5
6 protein backbone (Figure S3C). Thus, the potential physiological consequences of azole binding
7
8
9 to the DHP hemoglobin are two-fold: first, being directly bound to the heme-Fe, the azole could
10
11 possibly sterically hinder O₂-binding to a ferrous heme, and second, the distal histidine would
12
13 need to undergo substantial active site reorganization to effectively stabilize an oxyferrous
14
15 adduct. This is particularly noteworthy, as DHP already exhibits a much lower O₂ affinity ($K_{O_2} =$
16
17 3.23 μM) than observed for sperm whale myoglobin ($K_{O_2} = 0.27 \mu\text{M}$), a direct consequence that
18
19 arises from the need for the distal histidine in DHP, with a N^{α2}-Fe distance of 5.4 Å, to serve two
20
21 roles: dioxygen stabilization and acid/base catalyst.^{61, 62} By comparison, in globins the
22
23 corresponding distance is 4.1–4.6 Å⁶³ [e.g., human Hb: 4.24 Å (2W6V⁶⁴); equine hemoglobin:
24
25 4.35 Å (1NS9⁶⁵); sperm whale Mb: 4.61 Å (1BZP⁶⁶)], where it is well positioned to stabilize the
26
27 oxyferrous adduct formed upon O₂-binding to the ferrous heme. For peroxidases, the distance is
28
29 greater (5.5–6.0 Å), where the role of the distal histidine is to serve as the general acid/base
30
31 catalyst that facilitates H₂O₂ heterolysis, leading to enzyme activation. Thus, based on the results
32
33 from the present study, we suggest that azole binding has the potential to disrupt hemoglobin
34
35 function, although the effects of this possibility still need to be investigated in more detail.
36
37
38
39
40

41
42 The UV-visible and resonance Raman spectroscopic data are in excellent agreement with the
43
44 structural characterization of azole binding afforded by X-ray crystallography, and are well
45
46 supported by our computational work. Together, they provide strong evidence for the direct
47
48 binding of the azole ligand to the heme iron, leading to a hexacoordinate low-spin adduct.
49
50 Although not the direct subject of the present study, the physiological implications for marine
51
52 annelid survival are significant: taken together, the results suggest a new hypothesis where azole
53
54 pollutants can potentially disrupt hemoglobin function, and on this basis suggest a much larger
55
56
57
58
59
60

1
2
3 number of structurally related compounds may need to be re-evaluated as potential marine
4 environmental contaminants that pose significant health risks for aquatic organisms. Future
5 studies will focus on the evaluating the oxygen binding affinity of dehaloperoxidase as a function
6 of azole ligand, to further elucidate if this newly identified interaction represents a previously
7 unknown mode of toxicity.
8
9
10
11
12
13
14
15
16

17 ASSOCIATED CONTENT

19 **Supporting Information.** Optical spectra, titration curves, and resonance Raman spectra
20 (solution and single crystal) of DHP-azole complexes, data and refinement statistics for DHP B
21 ferric crystals complexed with azole ligands, and geometry optimized structures. This material is
22 available free of charge via the Internet at <http://pubs.acs.org>.
23
24
25
26
27
28
29
30
31

32 AUTHOR INFORMATION

33 Corresponding Authors

34 *Email: Reza_Ghiladi@ncsu.edu; Phone: 1-919-513-0680

35 *Email: mahough@essex.ac.uk; Phone: 44 1206 873317
36
37
38
39
40
41
42

43 Notes

44 The authors declare no competing financial interest.
45
46
47
48
49

50 ACKNOWLEDGMENT

51 This project was supported by NSF CAREER Award CHE-1150709 (R.G.), NSF CHE-1609446
52 (S.F. and R.G.), and Leverhulme Trust Project Grant RPG-2014-355 (T.M.C. and M.H.). We
53
54
55
56
57
58
59
60

1
2
3 thank Dr. Florian Dworkowski of the Paul Scherrer Institut/SLS for assistance with SCRR
4
5 measurements.
6
7
8
9

10 REFERENCES

- 11
- 12
- 13 1. Giger, W., Schaffner, C., and Kohler, H.-P. E. (2006) Benzotriazole and Tolyltriazole as
14 Aquatic Contaminants. 1. Input and Occurrence in Rivers and Lakes, *Environ. Sci.*
15 *Technol.* 40, 7186-7192.
- 16 2. Cancilla, D. A., Martinez, J., and van Aggelen, G. C. (1998) Detection of Aircraft
17 Deicing/Antiicing Fluid Additives in a Perched Water Monitoring Well at an
18 International Airport, *Environ. Sci. Technol.* 32, 3834-3835.
- 19 3. Weiss, S., Jakobs, J., and Reemtsma, T. (2006) Discharge of Three Benzotriazole
20 Corrosion Inhibitors with Municipal Wastewater and Improvements by Membrane
21 Bioreactor Treatment and Ozonation, *Environ. Sci. Technol.* 40, 7193-7199.
- 22 4. Reemtsma, T., Miehe, U., Duennbier, U., and Jekel, M. (2010) Polar pollutants in
23 municipal wastewater and the water cycle: Occurrence and removal of benzotriazoles,
24 *Water Res.* 44, 596-604.
- 25 5. Loos, R., Locoro, G., Comero, S., Contini, S., Schwesig, D., Werres, F., Balsaa, P., Gans,
26 O., Weiss, S., Blaha, L., Bolchi, M., and Gawlik, B. M. (2010) Pan-European survey on
27 the occurrence of selected polar organic persistent pollutants in ground water, *Water Res.*
28 44, 4115-4126.
- 29 6. Rodríguez, J. J. S., Padrón, M. E. T., Aufartová, J., and Ferrera, Z. S. (2010)
30 Benzimidazole Fungicides in Environmental Samples: Extraction and Determination
31 Procedures, In *Fungicides* (Carisse, O., Ed.), InTech.
- 32 7. Carlile, B. (2006) *Pesticide Selectivity, Health and the Environment*, Cambridge
33 University Press.
- 34 8. Hof, H. (2001) Critical Annotations to the Use of Azole Antifungals for Plant Protection,
35 *Antimicrob. Agents Chemother.* 45, 2987-2990.
- 36 9. Oh, S. J., Park, J., Lee, M. J., Park, S. Y., Lee, J.-H., and Choi, K. (2006) Ecological
37 hazard assessment of major veterinary benzimidazoles: Acute and chronic toxicities to
38 aquatic microbes and invertebrates, *Environ. Toxicol. Chem.* 25, 2221-2226.
- 39 10. Beynon, S. A. (2012) Potential environmental consequences of administration of
40 anthelmintics to sheep, *Vet. Parasitol.* 189, 113-124.
- 41 11. Gaikwad, D. D., Chapolikar, A. D., Devkate, C. G., Warad, K. D., Tayade, A. P., Pawar,
42 R. P., and Domb, A. J. (2015) Synthesis of indazole motifs and their medicinal
43 importance: An overview, *Eur. J. Med. Chem.* 90, 707-731.
- 44 12. Vandeputte, P., Ferrari, S., and Coste, A. T. (2012) Antifungal Resistance and New
45 Strategies to Control Fungal Infections, *Int. J. Microbiol.* 2012, 26 pages, Article ID
46 713687
- 47 13. Andersson Trojer, M., Movahedi, A., Blanck, H., and Nyden, M. (2013) Imidazole and
48 Triazole Coordination Chemistry for Antifouling Coatings, *J. Chem.* 2013, 23 pages,
49 Article ID 946739.
50
51
52
53
54
55
56
57
58
59
60

14. Forte, B., Malgesini, B., Piutti, C., Quartieri, F., Scolaro, A., and Papeo, G. (2009) A Submarine Journey: The Pyrrole-Imidazole Alkaloids, *Marine Drugs* 7, 705-753.
15. Reddy, C. M., Quinn, J. G., and King, J. W. (2000) Free and Bound Benzotriazoles in Marine and Freshwater Sediments, *Environ. Sci. Technol.* 34, 973-979.
16. Muirhead-Thomson, R. C. (2009) *Pesticide Impact on Stream Fauna: With Special Reference to Macroinvertebrates*, Cambridge University Press, Cambridge.
17. Weber, R. E., Mangum, C., Steinman, H., Bonaventura, C., Sullivan, B., and Bonaventura, J. (1977) Hemoglobins of two terebellid polychaetes: *Enoplobranchus sanguineus* and *Amphitrite ornata*, *Comp. Biochem. Physiol. A Comp. Physiol.* 56, 179-187.
18. Franzen, S., Thompson, M. K., and Ghiladi, R. A. (2012) The dehaloperoxidase paradox, *Biochim. Biophys. Acta* 1824, 578-588.
19. Lebioda, L., LaCount, M. W., Zhang, E., Chen, Y. P., Han, K., Whitton, M. M., Lincoln, D. E., and Woodin, S. A. (1999) An enzymatic globin from a marine worm, *Nature* 401, 445.
20. Franzen, S., Sasan, K., Sturgeon, B. E., Lyon, B. J., Battenburg, B. J., Gracz, H., Dumariah, R., and Ghiladi, R. (2012) Nonphotochemical base-catalyzed hydroxylation of 2,6-dichloroquinone by H₂O₂ occurs by a radical mechanism, *J. Phys. Chem. B* 116, 1666-1676.
21. D'Antonio, E. L., D'Antonio, J., de Serrano, V., Gracz, H., Thompson, M. K., Ghiladi, R. A., Bowden, E. F., and Franzen, S. (2011) Functional consequences of the creation of an Asp-His-Fe triad in a 3/3 globin, *Biochemistry* 50, 9664-9680.
22. Han, K., Woodin, S. A., Lincoln, D. E., Fielman, K. T., and Ely, B. (2001) *Amphitrite ornata*, a marine worm, contains two dehaloperoxidase genes, *Mar. Biotechnol. (NY)* 3, 287-292.
23. Barrios, D. A., D'Antonio, J., McCombs, N. L., Zhao, J., Franzen, S., Schmidt, A. C., Sombers, L. A., and Ghiladi, R. A. (2014) Peroxygenase and oxidase activities of dehaloperoxidase-hemoglobin from *Amphitrite ornata*, *J. Am. Chem. Soc.* 136, 7914-7925.
24. McCombs, N. L., D'Antonio, J., Barrios, D. A., Carey, L. M., and Ghiladi, R. A. (2016) Nonmicrobial Nitrophenol Degradation via Peroxygenase Activity of Dehaloperoxidase-Hemoglobin from *Amphitrite ornata*, *Biochemistry* 55, 2465-2478.
25. Franzen, S., Ghiladi, R. A., Lebioda, L., and Dawson, J. (2016) Chapter 10 Multi-functional Hemoglobin Dehaloperoxidases, In *Heme Peroxidases*, pp 218-244, The Royal Society of Chemistry.
26. Beers, R. F., Jr., and Sizer, I. W. (1952) A spectrophotometric method for measuring the breakdown of hydrogen peroxide by catalase, *J. Biol. Chem.* 195, 133-140.
27. Feducia, J., Dumariah, R., Gilvey, L. B., Smirnova, T., Franzen, S., and Ghiladi, R. A. (2009) Characterization of dehaloperoxidase compound ES and its reactivity with trihalophenols, *Biochemistry* 48, 995-1005.
28. D'Antonio, J., D'Antonio, E. L., Thompson, M. K., Bowden, E. F., Franzen, S., Smirnova, T., and Ghiladi, R. A. (2010) Spectroscopic and mechanistic investigations of dehaloperoxidase B from *Amphitrite ornata*, *Biochemistry* 49, 6600-6616.
29. Dumariah, R., D'Antonio, J., Deliz-Liang, A., Smirnova, T., Svistunenko, D. A., and Ghiladi, R. A. (2013) Tyrosyl Radicals in Dehaloperoxidase: How nature deals with

- 1
2
3
4
5
6
7
8
9
10
11
12
13
14
15
16
17
18
19
20
21
22
23
24
25
26
27
28
29
30
31
32
33
34
35
36
37
38
39
40
41
42
43
44
45
46
47
48
49
50
51
52
53
54
55
56
57
58
59
60
- evolving an oxygen-binding globin to a biologically relevant peroxidase, *J. Biol. Chem.* 288, 33470-33482.
30. Chenprakhon, P., Sucharitakul, J., Panijpan, B., and Chaiyen, P. (2010) Measuring Binding Affinity of Protein-Ligand Interaction Using Spectrophotometry: Binding of Neutral Red to Riboflavin-Binding Protein, *J. Chem. Educ.* 87, 829-831.
31. Pompidor, G., Dworkowski, F. S. N., Thominet, V., Schulze-Briese, C., and Fuchs, M. R. (2013) A new on-axis micro-spectrophotometer for combining Raman, fluorescence and UV/Vis absorption spectroscopy with macromolecular crystallography at the Swiss Light Source, *J. Synchrotron Radiat.* 20, 765-776.
32. Dworkowski, F. S. N., Hough, M. A., Pompidor, G., and Fuchs, M. R. (2015) Challenges and solutions for the analysis of in situ, in crystallo micro-spectrophotometric data, *Acta Crystallographica Section D: Biological Crystallography* 71, 27-35.
33. Kabsch, W. (2010) XDS, *Acta Crystallogr D Biol Crystallogr* 66, 125-132.
34. Evans, P. R., and Murshudov, G. N. (2013) How good are my data and what is the resolution?, *Acta Crystallogr D Biol Crystallogr* 69, 1204-1214.
35. Kleywegt, G. J. (2007) Crystallographic refinement of ligand complexes, *Acta Crystallogr D Biol Crystallogr* 63, 94-100.
36. Chen, V. B., Arendall, W. B., 3rd, Headd, J. J., Keedy, D. A., Immormino, R. M., Kapral, G. J., Murray, L. W., Richardson, J. S., and Richardson, D. C. (2010) MolProbity: all-atom structure validation for macromolecular crystallography, *Acta Crystallogr D Biol Crystallogr* 66, 12-21.
37. Zeldin, O. B., Gerstel, M., and Garman, E. F. (2013) RADDPOSE-3D: time- and space-resolved modelling of dose in macromolecular crystallography, *J. Appl. Crystallogr.* 46, 1225-1230.
38. Schäfer, A., Horn, H., and Ahlrichs, R. (1992) Fully optimized contracted Gaussian basis sets for atoms Li to Kr, *J. Chem. Phys.* 97, 2571-2577.
39. Ghiladi, R. A., Medzihradzky, K. F., Rusnak, F. M., and Ortiz de Montellano, P. R. (2005) Correlation between isoniazid resistance and superoxide reactivity in *Mycobacterium tuberculosis* KatG, *J. Am. Chem. Soc.* 127, 13428-13442.
40. Ghiladi, R. A., Medzihradzky, K. F., and Ortiz de Montellano, P. R. (2005) The role of the Met-Tyr-Trp crosslink in *Mycobacterium tuberculosis* catalase-peroxidase (KatG) as revealed by KatG(M255I), *Biochemistry* 44, 15093-15105.
41. Nienhaus, K., Deng, P., Belyea, J., Franzen, S., and Nienhaus, G. U. (2006) Spectroscopic study of substrate binding to the carbonmonoxy form of dehaloperoxidase from *Amphitrite ornata*, *J. Phys. Chem. B* 110, 13264-13276.
42. Nicoletti, F. P., Thompson, M. K., Howes, B. D., Franzen, S., and Smulevich, G. (2010) New insights into the role of distal histidine flexibility in ligand stabilization of dehaloperoxidase-hemoglobin from *Amphitrite ornata*, *Biochemistry* 49, 1903-1912.
43. Thompson, M. K., Davis, M. F., de Serrano, V., Nicoletti, F. P., Howes, B. D., Smulevich, G., and Franzen, S. (2010) Internal binding of halogenated phenols in dehaloperoxidase-hemoglobin inhibits peroxidase function, *Biophys. J.* 99, 1586-1595.
44. Belyea, J., Belyea, C. M., Lappi, S., and Franzen, S. (2006) Resonance Raman study of ferric heme adducts of dehaloperoxidase from *Amphitrite ornata*, *Biochemistry* 45, 14275-14284.

- 1
2
3
4 45. Deng, T. J., Proniewicz, L. M., Kincaid, J. R., Yeom, H., Macdonald, I. D., and Sligar, S.
5 G. (1999) Resonance Raman studies of cytochrome P450BM3 and its complexes with
6 exogenous ligands, *Biochemistry* 38, 13699-13706.
- 7 46. Smith, S. J., Munro, A. W., and Smith, W. E. (2003) Resonance Raman scattering of
8 cytochrome P450 BM3 and effect of imidazole inhibitors, *Biopolymers* 70, 620-627.
- 9 47. Macdonald, I. D., Smith, W. E., and Munro, A. W. (1996) Inhibitor/fatty acid interactions
10 with cytochrome P-450 BM3, *FEBS Lett.* 396, 196-200.
- 11 48. Davis, M. F., Gracz, H., Vendeix, F. A., de Serrano, V., Somasundaram, A., Decatur, S.
12 M., and Franzen, S. (2009) Different modes of binding of mono-, di-, and trihalogenated
13 phenols to the hemoglobin dehaloperoxidase from *Amphitrite ornata*, *Biochemistry* 48,
14 2164-2172.
- 15 49. Zhao, J., and Franzen, S. (2013) Kinetic study of the inhibition mechanism of
16 dehaloperoxidase-hemoglobin a by 4-bromophenol, *J. Phys. Chem. B* 117, 8301-8309.
- 17 50. Beitlich, T., Kuhnel, K., Schulze-Briese, C., Shoeman, R. L., and Schlichting, I. (2007)
18 Cryoradiolytic reduction of crystalline heme proteins: analysis by UV-Vis spectroscopy
19 and X-ray crystallography, *J. Synchrotron Radiat.* 14, 11-23.
- 20 51. Perutz, M. F. (1990) Mechanisms regulating the reactions of human hemoglobin with
21 oxygen and carbon monoxide, *Annu. Rev. Physiol.* 52, 1-25.
- 22 52. Zhao, J., de Serrano, V., Le, P., and Franzen, S. (2013) Structural and kinetic study of an
23 internal substrate binding site in dehaloperoxidase-hemoglobin A from *Amphitrite*
24 *ornata*, *Biochemistry* 52, 2427-2439.
- 25 53. Wang, C., Lovelace, L. L., Sun, S., Dawson, J. H., and Lebioda, L. (2013) Complexes of
26 dual-function hemoglobin/dehaloperoxidase with substrate 2,4,6-trichlorophenol are
27 inhibitory and indicate binding of halophenol to compound I, *Biochemistry* 52, 6203-
28 6210.
- 29 54. Locuson, C. W., Hutzler, J. M., and Tracy, T. S. (2007) Visible Spectra of Type II
30 Cytochrome P450-Drug Complexes: Evidence that "Incomplete" Heme Coordination Is
31 Common, *Drug Metab. Dispos.* 35, 614-622.
- 32 55. Hutzler, J. M., Melton, R. J., Rumsey, J. M., Schnute, M. E., Locuson, C. W., and
33 Wienkers, L. C. (2006) Inhibition of Cytochrome P450 3A4 by a Pyrimidineimidazole:
34 Evidence for Complex Heme Interactions, *Chem. Res. Toxicol.* 19, 1650-1659.
- 35 56. Alkorta, I., and Elguero, J. (2005) Theoretical estimation of the annular tautomerism of
36 indazoles, *J. Phys. Org. Chem.* 18, 719-724.
- 37 57. Chen, Z., de Serrano, V., Betts, L., and Franzen, S. (2009) Distal histidine conformational
38 flexibility in dehaloperoxidase from *Amphitrite ornata*, *Acta Cryst. D* 65, 34-40.
- 39 58. Smirnova, T. I., Weber, R. T., Davis, M. F., and Franzen, S. (2008) Substrate binding
40 triggers a switch in the iron coordination in dehaloperoxidase from *Amphitrite ornata*:
41 HYSORE experiments, *J. Am. Chem. Soc.* 130, 2128-2129.
- 42 59. de Serrano, V., D'Antonio, J., Franzen, S., and Ghiladi, R. A. (2010) Structure of
43 dehaloperoxidase B at 1.58 Å resolution and structural characterization of the AB dimer
44 from *Amphitrite ornata*, *Acta Cryst. D* 66, 529-538.
- 45 60. Zhao, J., de Serrano, V., Dumarieh, R., Thompson, M., Ghiladi, R. A., and Franzen, S.
46 (2012) The role of the distal histidine in H₂O₂ activation and heme protection in both
47 peroxidase and globin functions, *J. Phys. Chem. B* 116, 12065-12077.
- 48 61. Du, J., Huang, X., Sun, S., Wang, C., Lebioda, L., and Dawson, J. H. (2011) *Amphitrite*
49 *ornata* Dehaloperoxidase (DHP): Investigations of Structural Factors That Influence the
50
51
52
53
54
55
56
57
58
59
60

- 1
2
3
4
5
6
7
8
9
10
11
12
13
14
15
16
17
18
19
20
21
22
23
24
25
26
- Mechanism of Halophenol Dehalogenation Using “Peroxidase-like” Myoglobin Mutants and “Myoglobin-like” DHP Mutants, *Biochemistry* 50, 8172-8180.
62. Sun, S., Sono, M., Wang, C., Du, J., Lebioda, L., and Dawson, J. H. (2014) Influence of heme environment structure on dioxygen affinity for the dual function *Amphitrite ornata* hemoglobin/dehaloperoxidase. Insights into the evolutionary structure–function adaptations, *Arch. Biochem. Biophys.* 545, 108-115.
63. Matsui, T., Ozaki, S., Liong, E., Phillips, G. N., Jr., and Watanabe, Y. (1999) Effects of the location of distal histidine in the reaction of myoglobin with hydrogen peroxide, *J. Biol. Chem.* 274, 2838-2844.
64. Savino, C., Miele, A. E., Draghi, F., Johnson, K. A., Sciara, G., Brunori, M., and Vallone, B. (2009) Pattern of cavities in globins: The case of human hemoglobin, *Biopolymers* 91, 1097-1107.
65. Robinson, V. L., Smith, B. B., and Arnone, A. (2003) A pH-Dependent Aquomet-to-Hemichrome Transition in Crystalline Horse Methemoglobin, *Biochemistry* 42, 10113-10125.
66. Kachalova, G. S., Popov, A. N., and Bartunik, H. D. (1999) A Steric Mechanism for Inhibition of CO Binding to Heme Proteins, *Science* 284, 473-476.

27
28
29
30
31
32
33
34
35
36
37
38
39
40
41
42
43
44
45
46
47
48
49
50
51
52
53
54
55
56
57
58
59
60

TOC Graphic (For Table of Contents Only)

